Sequoia Andrade*, Danika Heaney**,
Ron Cohen**, Ryan Giordano*
*Department of Statistics, **College of Chemistry
University of California, Berkeley
srandrade@berkeley.edu

Posterior Uncertainty and Model Diagnostics for Large Scale Carbon Emission Monitoring

Introduction

- The atmosphere is composed of various gasses – for example CO_2, O_2, NO, CH_4 – some are "greenhouse gases" (GHG)
- Anthropogenic climate change is associated with human-produced GHGs, such as fossil fuel burning and agriculture, which needs to be quantified to monitor emissions goals [1]
- Berkeley Environmental Air Quality and CO_2 Network (BEACO_2N) is a 2km dense in-situ network of ground-based sensors clustered over city centers that collects information on 6 gasses and particulate matter [2]
- Previous research has used BEACO_2N sensors and a Bayesian linear atmospheric inversion model [3] to monitor emissions trends [1,4]
- In this work, we analyze posterior uncertainty, model performance, and model sensitivity, applying established statistical methods to carbon emissions monitoring for the first time

Linear Atmospheric Inversion Model

- The forward model represents sensor readings, $\boldsymbol{y} \in \mathbb{R}^{n}$, as a function of emissions, $\boldsymbol{x} \in \mathbb{R}^{(96\times127\times137)}$, linearly transported via atmospheric dynamics represented by matrix $\boldsymbol{H} \in \mathbb{R}^{n\times(96\times127\times137)}$:

$$\boldsymbol{y} = \boldsymbol{Hx} + \boldsymbol{\epsilon}$$
$$\boldsymbol{y}|\boldsymbol{x} \sim N(\boldsymbol{Hx}, \boldsymbol{R})$$

- Prior emissions, $\boldsymbol{x}$, are normally distributed with mean $\boldsymbol{x_a}$ and covariance $\boldsymbol{B}$, where $\boldsymbol{B}$ is a spatial-temporal Kronecker product [5] of $\boldsymbol{S_t} \in \mathbb{R}^{96\times96}$ (Fig. 2) and $\boldsymbol{S_{xy}} \in \mathbb{R}^{(127\times137)\times(127\times137)}$ (Fig. 1):

$$\boldsymbol{x} \sim N(\boldsymbol{x_a}, \boldsymbol{B})$$
$$\boldsymbol{B} = \boldsymbol{S_t} \otimes \boldsymbol{S_{xy}}$$

- Then jointly we have:

$$\begin{pmatrix}\boldsymbol{x}\\ \boldsymbol{y}\end{pmatrix} \sim \boldsymbol{N}\left(\begin{matrix}\boldsymbol{x_a}\\ \boldsymbol{Hx_a}\end{matrix}, \begin{pmatrix}\boldsymbol{B} & \boldsymbol{HB^T}\\ \boldsymbol{HB} & \boldsymbol{HBH^T} + \boldsymbol{R}\end{pmatrix}\right)$$

- The posterior of emissions (Fig. 3) is then given by :

$$\boldsymbol{x}|\boldsymbol{y} \sim N(\hat{\boldsymbol{x}}, \hat{\boldsymbol{\Sigma}})$$
$$\hat{\boldsymbol{x}} = \boldsymbol{x_a} + (\boldsymbol{HB})^{\boldsymbol{T}}\left(\boldsymbol{HBH^T} + \boldsymbol{R}\right)^{-1}(\mathrm{y} - \boldsymbol{Hx_a})$$
$$\hat{\boldsymbol{\Sigma}} = \boldsymbol{B} + (\boldsymbol{HB})^{\boldsymbol{T}}\left(\boldsymbol{HBH^T} + \boldsymbol{R}\right)^{-1}\boldsymbol{HB}$$

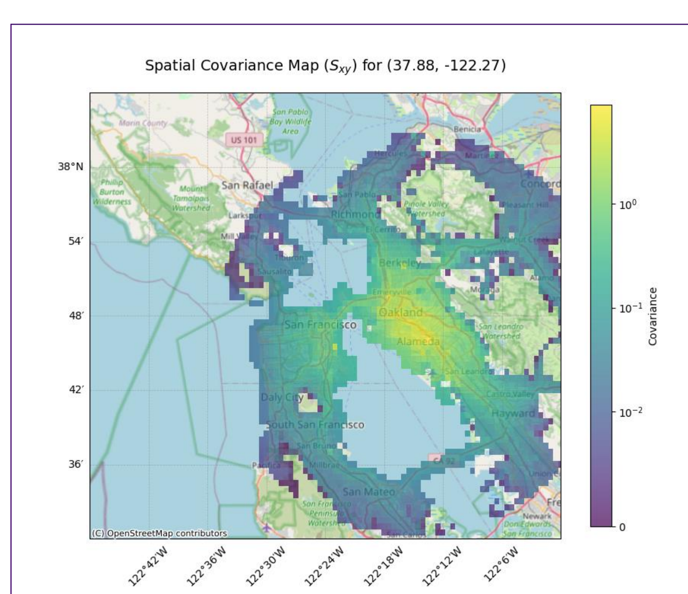

Figure 1: Example prior spatial covariance for a single location, corresponding to a row of S_{xy}

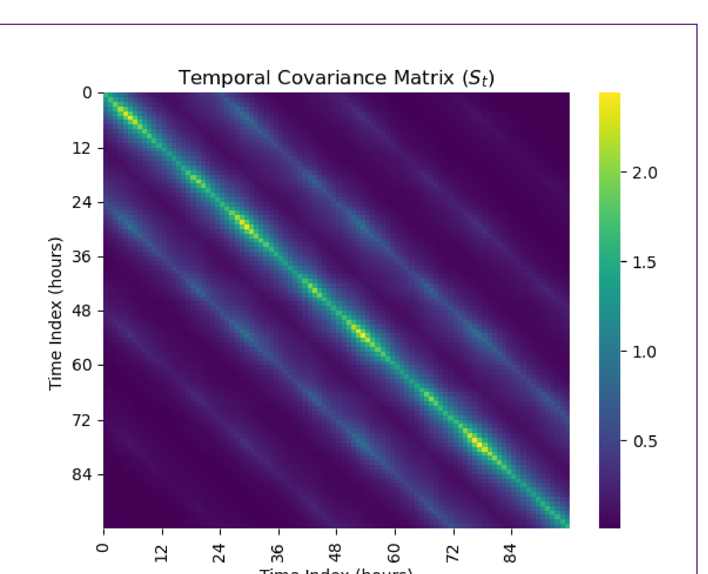

Figure 2: Example temporal covariance S_t

Results

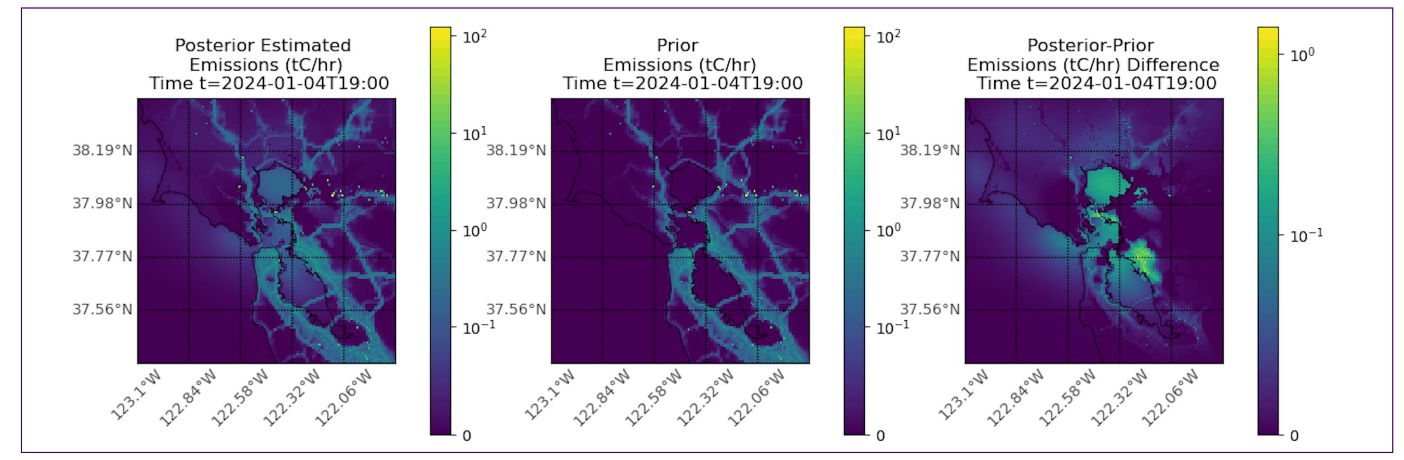

Figure 3: Example posterior, prior, and difference between posterior and prior

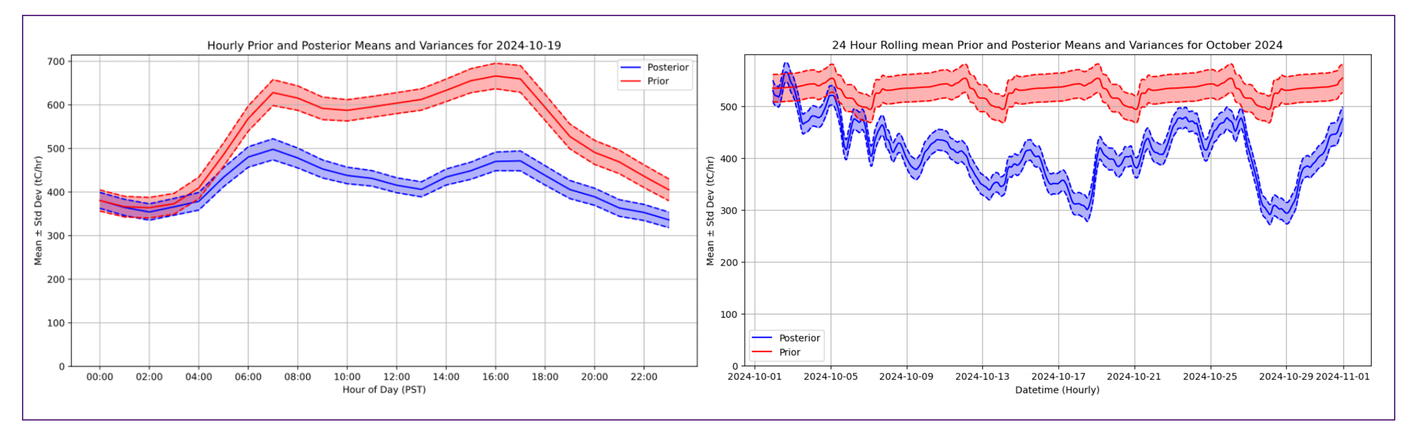

Figure 4: Example posterior mean and variance diurnal (left) and monthly (right) trends

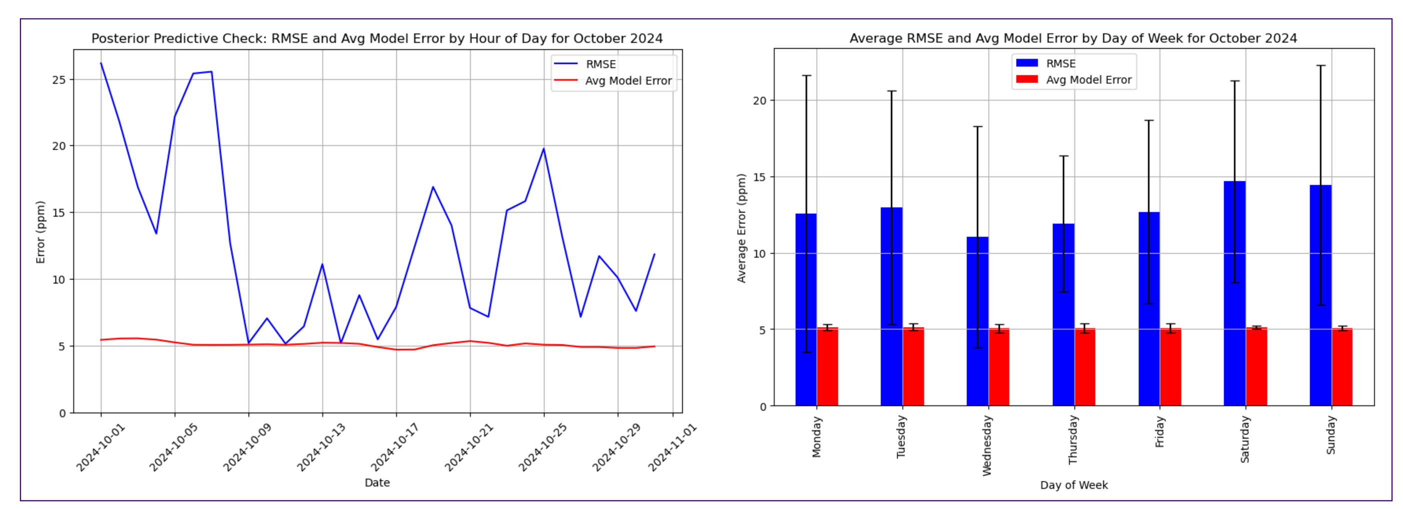

Figure 5. Observed daily model error and aggregated day of the week error over one month of inversions compared to expected average model error

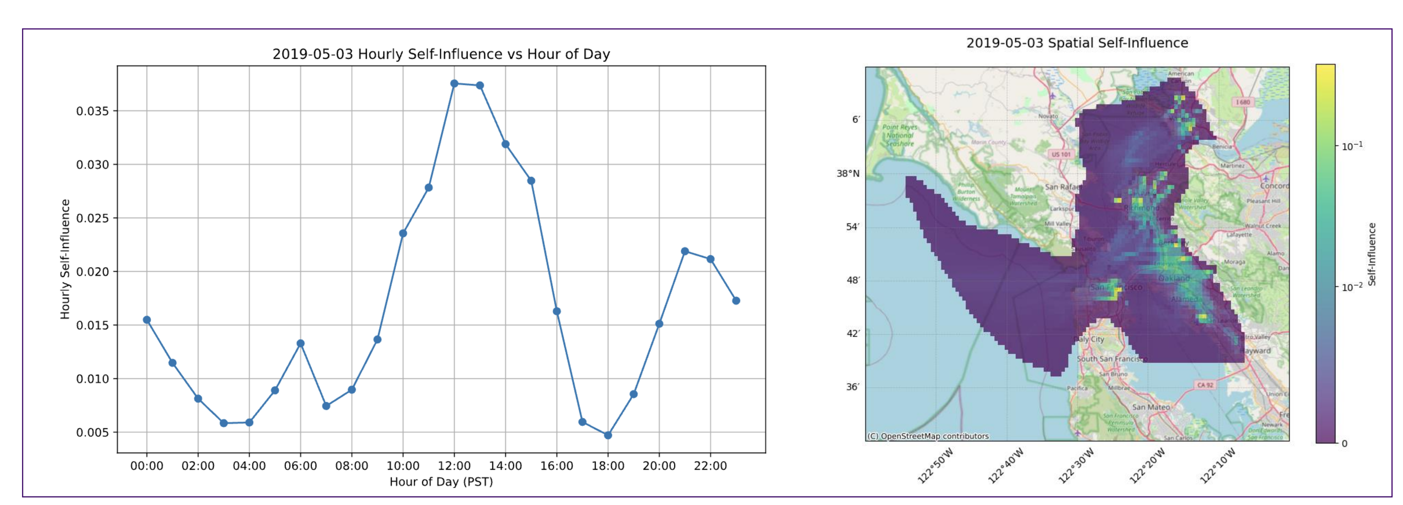

Figure 6. Hourly self-influence and spatial self-influence

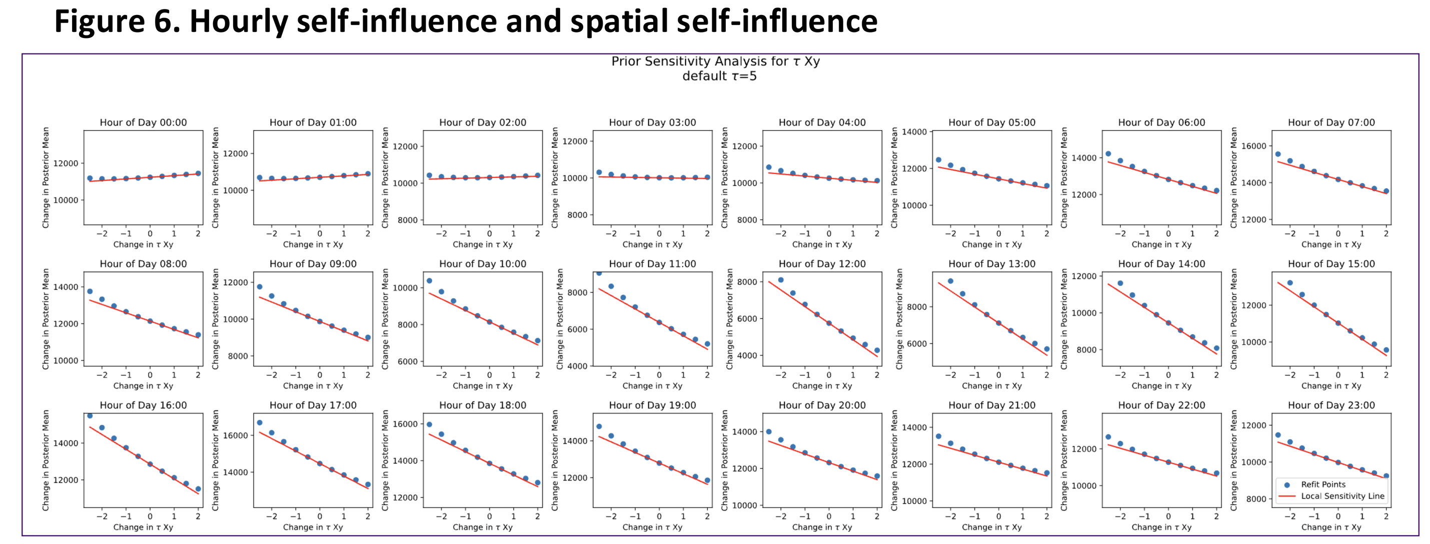

Figure 7. Local prior hyper parameter sensitivity with refits across spatial smoothing prior covariance hyperparameter

Posterior Variance

- Existing analyses do not compute the posterior variance and deem it intractable; however, size-reducing linear combinations of the posterior variance are tractable (see Fig. 4)
- Typical analyses are interested in total hourly emissions, which we can calculate the posterior variance for by representing hours of interest via a matrix, $A^T \in \mathbb{R}^{24\times(96\times127\times137)}$:

$$A^T\,\hat{\Sigma}A = \underbrace{A^TBA}_{24\text{x}24} - \underbrace{A^T(HB)^T}_{24\text{x n}}\underbrace{(HBH^T + R)^{-1}}_{\text{nxn}}\underbrace{HBA}_{\text{nx}24}$$

Posterior Predictive Check

- Given a posterior mean $\hat{\boldsymbol{x}}$, evaluate the model fit by considering (Fig. 5):

$$\hat{\mathrm{Y}} = \mathrm{H}\hat{\mathrm{x}}$$
$$MSE = \frac{1}{nt}\sum_{i=1}^{nt}\left(Y_i - \hat{Y}_i\right)^2 = \frac{1}{nt}\left(Y - \hat{Y}\right)^T\left(Y - \hat{Y}\right),\ \mathrm{RMSE} = \sqrt{\mathrm{MSE}}$$

Self-Influence Functions

- Identify if small changes, Δ, in a segment, can be detected (Fig. 6)
- Define:

$$\boldsymbol{x}(\Delta) = \boldsymbol{x} + \Delta,\qquad \boldsymbol{Y}(\Delta) = \boldsymbol{H}(\boldsymbol{x} + \Delta),\qquad \hat{\boldsymbol{x}}(\Delta) = \hat{\boldsymbol{x}} + \frac{\boldsymbol{d}\hat{\boldsymbol{x}}(\Delta)}{\boldsymbol{d}\Delta}\Delta + \boldsymbol{\varepsilon}$$
$$\frac{\boldsymbol{d}\hat{\boldsymbol{x}}(\Delta)}{\boldsymbol{d}\Delta} = \frac{\boldsymbol{d}\hat{\boldsymbol{x}}(\Delta)}{\boldsymbol{dY}(\Delta)}\frac{\boldsymbol{dY}(\Delta)}{\boldsymbol{d}\Delta} = (\boldsymbol{HB})^{\boldsymbol{T}}\left(\boldsymbol{HBH^T} + \boldsymbol{R}\right)^{-1}\boldsymbol{H} = \boldsymbol{GH}$$

- Consider the ratio of the change of the posterior to the change in the prior, for some sets of points defined by matrix A :

$$\frac{A^T(\hat{\boldsymbol{x}}(\Delta) - \hat{\boldsymbol{x}})A}{A^T(\boldsymbol{x}(\Delta) - \boldsymbol{x})A} = \frac{A^T((\hat{\boldsymbol{x}} + \boldsymbol{GH}\Delta) - \hat{\boldsymbol{x}})A}{A^T((\boldsymbol{x} + \Delta) - \boldsymbol{x})A} = \frac{A^T\mathrm{GH}A}{A^TA}$$

Prior Hyperparameter Sensitivity

- The prior covariance is a function of smoothing hyperparameters, τ
- We can use local sensitivity to examine how small changes to the smoothing hyperparameters impacts the posterior by considering the derivative:

$$\frac{d\hat{\boldsymbol{x}}}{d\tau} = \frac{d}{d\tau}\left(\boldsymbol{x_a} + (\boldsymbol{HB(\tau)})^{\boldsymbol{T}}\left(\boldsymbol{HB(\tau)H^T} + \boldsymbol{R}\right)^{-1}(\boldsymbol{y} - \boldsymbol{Hx_a})\right)$$

- We compare the estimated local sensitivity to actual refits (Fig. 7)

Conclusions

- Posterior emissions are consistently lower than prior emissions inventories
- Observed error tends to be higher than expected given the model, indicating underestimation of uncertainty in the marginal $\boldsymbol{y}|\boldsymbol{x} \sim N(\boldsymbol{Hx}, \boldsymbol{R})$
- Midday sensor readings are the most sensitive to real-world changes
- Spatial locations closer to sensors are more sensitive to real-world changes
- Increasing smoothing parameters decreases hourly emissions estimates

References

[1] N. Asimow, A. Turner, and R. Cohen. Sustained Reductions of Bay Area CO2 Emissions 2018–2022. 58(15):6586–6594. ISSN 0013-936X. doi: 10.1021/acs.est.3c09642. URL https://doi.org/10.1021/acs.est.3c09642

[2] BEACO2N Network. Beaco2n: A network of atmospheric co2 and ch4 measurements. https://beacon.berkeley.edu/about/ , 2025. Accessed: 2025-07-17

[3] Andrew Bennett. Inverse modeling of the ocean and atmosphere. Cambridge University Press, 2005.

[4] A. Turner, J. Kim, H. Fitzmaurice, C. Newman, K. Worthington, K. Chan, P. Wooldridge, P. K¨oehler, C. Frankenberg, and R. Cohen. Observed Impacts of COVID-19 on Urban CO Emissions. 47(22):e2020GL090037, 2020. ISSN1944-8007. doi: 10.1029/2020GL090037.

[5] Yadav, V. and Michalak, A. M.: Improving computational efficiency in large linear inverse problems: an example from carbon dioxide flux estimation, Geosci. Model Dev., 6, 583–590, https://doi.org/10.5194/gmd-6-583-2013, 2013.